Global network modulation during thalamic stimulation for Tourette syndrome

Hang Joon Jo[a,b], Kevin W. McCairn[c], William S. Gibson[a], Paola Testini[a], Cong Zhi Zhao[b],
Krzysztof R. Gorny[d], Joel P. Felmlee[d], Kirk M. Welker[d], Charles D. Blaha[a], Bryan T. Klassen[b],
Hoon-Ki Min[a,d,e,*], Kendall H. Lee[a,e,*]

[a] Department of Neurologic Surgery, Mayo Clinic, Rochester, MN 55905, USA
[b] Department of Neurology, Mayo Clinic, Rochester, MN 55905, USA
[c] Systems Neuroscience Section, Primate Research Institute, Kyoto University, Inuyama, Aichi 484-8506, Japan
[d] Department of Radiology, Mayo Clinic, Rochester, MN 55905, USA
[e] Department of Physiology and Biomedical Engineering, Mayo Clinic, Rochester, MN 55905, USA

ARTICLE INFO

ABSTRACT

Background and objectives: Deep brain stimulation (DBS) of the thalamus is a promising therapeutic alternative for treating medically refractory Tourette syndrome (TS). However, few human studies have examined its mechanism of action. Therefore, the networks that mediate the therapeutic effects of thalamic DBS remain poorly understood.

Methods: Five participants diagnosed with severe medically refractory TS underwent bilateral thalamic DBS stereotactic surgery. Intraoperative fMRI characterized the blood oxygen level-dependent (BOLD) response evoked by thalamic DBS and determined whether the therapeutic effectiveness of thalamic DBS, as assessed using the Modified Rush Video Rating Scale test, would correlate with evoked BOLD responses in motor and limbic cortical and subcortical regions.

Results: Our results reveal that thalamic stimulation in TS participants has wide-ranging effects that impact the frontostriatal, limbic, and motor networks. Thalamic stimulation induced suppression of motor and insula networks correlated with motor tic reduction, while suppression of frontal and parietal networks correlated with vocal tic reduction. These regions mapped closely to major regions of interest (ROI) identified in a nonhuman primate model of TS.

Conclusions: Overall, these findings suggest that a critical factor in TS treatment should involve modulation of both frontostriatal and motor networks, rather than be treated as a focal disorder of the brain. Using the novel combination of DBS-evoked tic reduction and fMRI in human subjects, we provide new insights into the basal ganglia-cerebellar-thalamo-cortical network-level mechanisms that influence the effects of thalamic DBS. Future translational research should identify whether these network changes are cause or effect of TS symptoms.

1. Introduction

Often presenting a constellation of unusual repetitive movement and vocalization behaviors, Tourette syndrome (TS) is a complex, developmental neuropsychiatric disorder. In many cases, it generally resolves with maturation, however, severe cases can persist into adulthood and can have a serious impact on patient quality of life and medical resources (Crossley and Cavanna, 2013). Clinically, TS is defined by persistent stereotypic motor and vocal tics, and by pre-tic premonitory urges or compulsions (Albin and Mink, 2006; Hallett, 2001; McGuire et al., 2016). The combination of motor and neuropsychiatric symptoms (Cavanna et al., 2017), suggests that the pathophysiology of TS is mediated by dysregulation of the basal ganglia-cerebellar-thalamo-cortical (BGCTC) networks, involving frontal, limbic and motor areas of the basal ganglia (BG) (Caligiore et al., 2017; Hallett, 2015; Krack et al., 2010). In support of both motor and limbic BG circuitry involvement in tic generation, utilizing in vivo electrophysiology and imaging, McCairn et al. found that in nonhuman primates (NHP), focal disinhibition of putamen (PT) and nucleus accumbens (NAc) can induce myoclonic (motor) and vocal (limbic) tics, respectively (McCairn et al., 2016). This led to the suggestion that, despite BG-located focal abnormalities, TS-like states should be

considered as functionally specific, global network dysrhythmias (McCairn et al., 2009, 2013b, 2016).

For participants with severe, medically refractory TS, deep brain stimulation (DBS) is increasingly considered a viable option (Ackermans et al., 2011; Maciunas et al., 2007; Testini et al., 2016b; Vandewalle et al., 1999). DBS is thought to relieve symptoms of conditions by applying relatively small amplitude electrical stimulation to dysfunctional brain networks and modulating pathological brain activity at the stimulation target site with up and downstream network effects playing a prominent role (Da Cunha et al., 2015; Kringelbach et al., 2007; McCairn et al., 2015). DBS of the thalamus has been reported to alleviate both motor and vocal tics in TS (Huys et al., 2016), but its therapeutic and network mechanisms remain unknown.

Located in the posterior intralaminar thalamus, the centromedian and parafascicularis complex (CMPf) is uniquely situated to modulate both motor and limbic networks (Eckert et al., 2012; Kim et al., 2013; Sadikot and Rymar, 2009) and has thus been considered a viable DBS target for TS (Testini et al., 2016b). As part of the diffuse thalamocortical projection system, the CMPf sends direct neuronal projections to limbic areas, including amygdala (AM) (Ottersen, 1981), hippocampus (HP) (Cavdar et al., 2008), anterior cingulate cortex (ACC), and insula (Eckert et al., 2012; Van der Werf et al., 2002). The CMPf also has extensive projections throughout the striatum (caudate/PT), NAc, and globus pallidus (Berendse and Groenewegen, 1991; Eckert et al., 2012; Jayaraman, 1985; Macchi et al., 1984). The CMPf complex of thalamus provides unique access to both motor and limbic networks that has been shown to be related to complex tic behaviors in NHP-TS models (McCairn et al., 2016).

Here, we address the proposed global network dysrhythmia hypothesis as inferred from NHP-TS studies by determining correlates of brain wide activity induced by DBS using high frequency stimulation (HFS) of the thalamus (CMPf) with reductions in TS symptoms (motor and vocal tics). DBS surgery was performed on participants with severe medically-refractive TS who exhibited complex motor and vocal tics. Thereafter, BGCTC network properties were assessed using intraoperative (intra-OR) functional magnetic resonance imaging (fMRI) during thalamic HFS. This method has been previously used for thalamic HFS in essential tremor subjects (Gibson et al., 2016). Intra-OR fMRI results were correlated with post-operative behavioral scores to measure tic frequency, severity, and impairment levels in which participants and judges were blinded to stimulation parameters (Goetz et al., 1999; Huys et al., 2016). To further separate the possible intercorrelation effects between vocal and motor tic reduction, standard and partial correlation methods were used to separate out the unique portions of variation in each behavioral measure that were associated with fMRI blood-oxygen level dependent (BOLD) signal changes.

2. Materials and methods

2.1. Participants

This study included five participants (2 females, 3 males; mean age of 27 years) conducting a total of 25 fMRI scans with 12 tic behavioral score tests. The participants diagnosed with TS underwent bilateral CMPf DBS stereotactic surgery. The diagnosis of TS was based on the DSM-5307.22 diagnostic criteria for chronic motor and vocal (phonic) tic disorder (Association, 2013). All participants were approved for surgery by the Mayo Clinic DBS Committee, which is composed of neurologists, neurosurgeons, psychiatrists, neuropsychologists, speech pathologists, and a biomedical ethicist. In all participants, TS symptoms predominantly affected the bilateral upper extremities with both simple and complex motor and vocal (phonic) tic, and in some participant's tremor also affected the head, jaw, and/or voice (Table S1). This study was approved by the Mayo Clinic Institutional Review Board, and all participants provided written informed consent. Clinical trial name and number: Functional Magnetic Resonance Imaging During Deep Brain

Stimulation (DBS) to Treat Parkinson's Disease - NCT01809613; URL: https://clinicaltrials.gov/ct2/show/NCT01809613

2.2. Surgical approach

Each participant was secured within the Leksell™ stereotactic head frame (Elekta, Stockholm, Sweden) and a 1.5 T structural MRI (General Electric Signa HDx and 16× software) scan was performed prior to implantation using magnetization-prepared rapid acquisition gradient-echo (MP-RAGE) sequence (Gibson et al., 2016). The MRI data were merged with a stereotaxy human brain atlas (Schaltenbrand and Wahren, 1977), and stereotactic coordinates were identified for the CMPf thalamic complex (9.5–11.0 mm posterior, 5.0–7.0 mm lateral, 1.5–3.0 mm inferior to the mid AC-PC line). Quadripolar 3387 dB leads (Medtronic, Minneapolis, MN) were implanted bilaterally and lead placement was confirmed by computed tomography (Sensation 64, Siemens): image resolution: $0.59 \times 0.59 \times 1.00\,mm^3$. With reference to a functional probabilistic human brain atlas (Eickhoff et al., 2007), post-hoc analysis of CT-MR fusion data of the region of thalamus occupied by the DBS lead electrode contacts implanted confirmed that they were centered on prefrontal and premotor thalamus (Supplementary Fig. S2).

2.3. Intraoperative functional MRI

The intra-OR fMRI experiment was performed during pulse generator implantation surgery, 1 week after the DBS lead implantation surgery (for detailed methods, see (Gibson et al., 2016)). After general anesthesia induction, a unilateral (right side) DBS lead was externalized under sterile conditions and attached to a custom wire connected to an external pulse generator (DualScreen 3628, Medtronic, Minneapolis, MN) outside the sterile field. To minimize the effects of susceptibility artifacts produced by subgaleal connectors, the laterality (right in five participants) of the connected lead was selected such that it was contralateral to the implantable pulse generator (Knight et al., 2015). Participants were then moved into the magnet bore and all scans were conducted with participants under general anesthesia (Gibson et al., 2016). Average head specific absorption rate (SAR) values of < 0.1 W/ kg were recorded during the fMRI study in all the participants, and a board-certified MRI physicist was present during all the sessions (Gorny et al., 2013). An anesthesia team was also present during all sessions and vital signs were continuously monitored. For all sequences, a manufacturer's standard transmit/receive RF head coil was used (1.5-T quadrature head coil, model 46-28211862; GE Healthcare, Maple Grove, MN). The fMRI was acquired using 2-dimensional gradient echo-echo planar imaging (GE-EPI): repetition time/echo time, 3000/50; flip angle, 90°; field of view, 22×22 cm; matrix, 64×64; slice thickness, 3.5 mm with a 0-mm gap thickness. For each acquisition, 135 volumes (the first five volumes were discarded for scanner equilibration) were acquired using a block paradigm, with five 6 s stimulation periods (two volumes) alternated with six 60 s rest periods (20 volumes), for a total time of 6 min 45 s per run. A total of 25 fMRI runs were collected, with each participant undergoing 4–6 runs of fMRI in a single session with 2 min of rest between each run. Four runs were consistent across all five participants. Bipolar thalamic HFS (90 μs width, 130 Hz, +3 V) was applied to the right DBS lead with the following contact configurations: 0–1+, 2–3+ with minimum of two repetitions for the same contact configuration. By convention, contact '0' refers to the most ventrally-located contact on the quadripolar DBS lead, contact '3' is the most dorsally-located. The cathode or current source is denoted by '−', and '+' refers to the passive/return contact. Following fMRI, participants were returned to the operating room for pulse generator implantation.

2.4. Tic score evaluation

After three months of active bilateral DBS of the CMPf, four out of
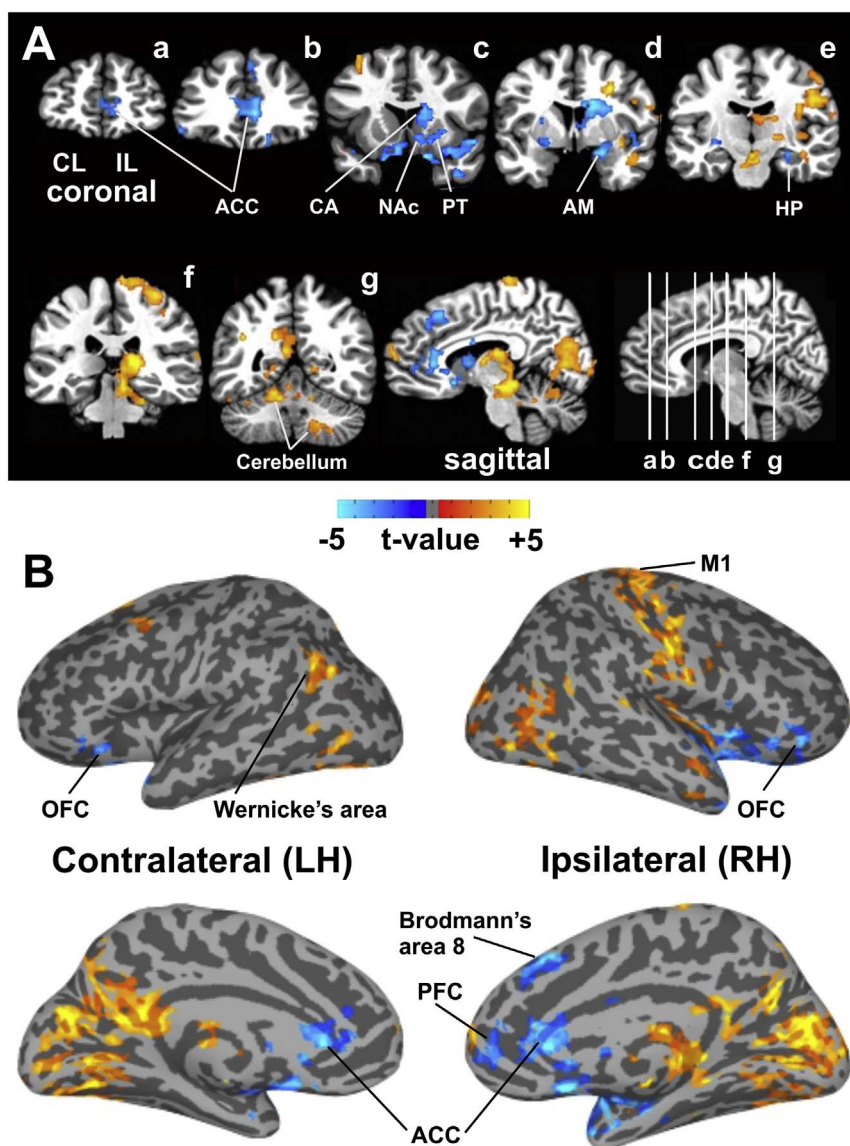
Fig. 1. Intraoperative fMRI during thalamic HFS. (A) Thalamic HFS showing both significant (FWE-correct p < 0.05) increases and decreases in BOLD activation in a number of network areas: 1) frontal: PFC, ACC, and OFC; 2) motor: sensorimotor cortex and cerebellum; 3) BG and thalamic regions; 4) limbic: AM, NAc, insula, and temporal lobe, including the parahippocampal gyrus in the medial temporal lobe; and 5) parietal and occipital lobes. (B) Brain cortical surface maps confirm increases in BOLD activity in the M1 that includes the entire motor strip (IL/RH), both increases and decreases in BOLD in the PFC (IL/RH), and decreases in BOLD in the ACC and OFC in both hemispheres. Decreases in BOLD were also found in the medial frontal cortex, including Brodmann's area 8 (IL/RH), increases in BOLD in the inferior parietal cortex (CL/LH), which includes Wernicke's area, and a wide range of increased BOLD activation in the parietal and occipital lobes in both hemispheres. See Fig. S3 and S4 for gray matter and white matter surface maps for anatomical confirmation. Abbreviations: ACC, anterior cingulate cortex; AM, amygdala; BG, basal ganglia; CA, caudate; HP, hippocampus; M1, primary motor cortex; NAc, nucleus accumbens; OFC, orbitofrontal cortex; PFC, prefrontal cortex; PT, putamen; BOLD, blood-oxygen-level dependent; fMRI, functional magnetic resonance imaging; FWE, family-wise error; HFS, high frequency stimulation; CL/LH, contralateral to the stimulation site at the left hemisphere; IL/RH, ipsilateral to the stimulation site at the right hemisphere; LH, left hemisphere; RH, right hemisphere.

five participants (one declined to participate) underwent the Modified Rush Video Rating Scale (mRVRS) test that allows double-blinded objective tic assessments (Goetz et al., 1999; Huys et al., 2016). Each participant was blinded as to the stimulation settings, and underwent programming to three settings in succession, in a randomized order (n = 12): sham DBS (off), dorsal contact DBS (bilateral; 2–3+; +3 V; 130 Hz; 90 μs), and ventral contact DBS (bilateral; 0–1+; +3 V; 130 Hz; 90 μs). During application of each stimulation setting, participants underwent 10 min of videotaping according to the mRVRS protocol. In brief, participants were placed in front of a video camera in a quiet room, and full frontal body (5 min) as well as close-up head and shoulder views (5 min) were recorded. Five domains were evaluated by a neurologist blinded to the conditions with subspecialty training in movement disorders: number of body areas involved with tics, motor tic intensity, vocal tic intensity, frequency of motor tics, and frequency of vocal tics. Reductions in mRVRS scores relative to sham stimulation (⊿mRVRS; positive values representing reductions in score) were evaluated by Wilcoxon Signed Rank test.

2.5. Functional MRI processing

FMRI data were preprocessed and analyzed using AFNI (Analysis of Functional NeuroImages; http://afni.nimh.nih.gov) software packages

(Cox, 1996). The T1 anatomical image was aligned to the fifth volume of the EPI time series by affine registration using a local Pearson correlation cost function (Saad et al., 2009). The first four volumes of the time series were removed to ensure that all remaining volumes in the time-series were at magnetization steady state. Despiking and rigid body registration were used to estimate subject movement during EPI scans and to correct for slice acquisition timing (Cox and Jesmanowicz, 1999). In all participants, estimated displacement due to head motion was < 0.5 mm in any given axis between successive time series volumes. The time series were then spatially transformed to the Talairach N27 brain template (Holmes et al., 1998) via affine transformation matrices estimated by registering T1-images to the N27 template. The spatially normalized EPI data were intensity scaled, and smoothed by a typical Gaussian blur of 4 mm full-width at half-maximum. At the individual session level, the general linear model estimated the shape of the hemodynamic response with respect to the timing of stimulation. To account for baseline drift and residual motion artifact, regressors included six motion parameters estimated during co-registration and a third-order baseline drift function. A regressor was created for the above-mentioned blocked stimulation paradigm, and convolved with a gamma-variate hemodynamic response function. Following the general linear model process, 25 beta-coefficient maps were obtained for the entire subject group. To obtain the stimulation-evoked activation map,

a group-level linear mixed-effects model was conducted to adjust for within-subject activation baselines, age, DBS contact, and voltage effects (Chen et al., 2014; Gibson et al., 2016; Gotts et al., 2013). To confirm cortical ROIs, brain surface maps were created by performing cortical parcellation (Fischl, 2012).

2.6. Correlation between stimulation-evoked BOLD signal and tic reduction

For correlation analysis, regions of interest (ROIs) were defined from the group activation map threshold at a significance level of family-wise error (FWE)-corrected $p < 0.05$ (two-tailed; $|t| > 2.15$; cluster size $> 840\ cm^3$). Beta coefficients were extracted from individual activation maps, averaged within each ROI to determine Pearson correlations between ROI-averaged beta values and the ⊿mRVRS scores. In addition, individual voxels were identified that exhibited correlations between beta coefficient values and ⊿mRVRS scores. For this analysis, a Monte Carlo simulation indicated that an initial, voxel-wise threshold of FWE-corrected $p < 0.05$ was applied. As a final analysis, vocal and motor tic reduction scores were separated in the mRVRS score, and standard and partial correlation methods were applied to separate out the unique portions of variation in each measure that were associated with the BOLD signal changes.

3. Results

3.1. Thalamic HFS modulated brain areas that are relevant to tic generation

Intra-OR fMRI during thalamic HFS showed both increased and decreased BOLD activation in BG-thalamic and cortical motor and limbic network areas. These regions mapped closely to major region of interest (ROI) identified in the NHP-TS model related to tic generation (McCairn et al., 2016; supplementary Fig. S1). Thalamic HFS resulted in significant (FWE-corrected $p < 0.05$) BOLD signal changes across a wide range of brain networks: 1) frontal, including prefrontal cortex (PFC) and medial and lateral orbitofrontal cortex (OFC), and the ACC, 2) motor, including sensorimotor cortex and cerebellum; 3) BG and thalamic regions; 4) limbic, including AM, NAc, insula, and temporal lobe, including the parahippocampal gyrus in the medial temporal lobe; and 5) parietal and occipital lobes (Fig. 1A and Table 1).

Brain cortical surface maps confirmed thalamic HFS-induced increases in BOLD activity in the primary motor cortex (M1) that included the entire motor strip. Changes in BOLD, both increases and decreases, were observed in the PFC ipsilateral to the stimulation site in the right hemisphere (IL/RH), and decreases in BOLD in the ACC and OFC in both hemispheres. This included decreases in BOLD in the medial frontal cortex, as well as Brodmann's area 8 (IL/RH) that involves complex movement planning. In addition, increases in BOLD were also found in the inferior parietal cortex in the contralateral, left hemisphere (CL/LH), which included Wernicke's area. The surface map also confirmed a wide range of increases in BOLD activation in the parietal and occipital lobes in both hemispheres (Fig. 1B).

3.2. Neural correlates of tic reduction by thalamic HFS

Participants receiving thalamic HFS during clinical evaluation exhibited a significant reduction in tics (mean mRVRS score of 5.38 SEM ± 1.14) compared to participants receiving sham stimulation (mean mRVRS score of 7.25 SEM ± 1.98) (Wilcoxon signed rank test $p < 0.05$) (Fig. 2A).

Reductions in mRVRS score during thalamic HFS relative to sham stimulation (⊿mRVRS; positive values representing reductions in score) were used to correlate with the change in fMRI BOLD signal during thalamic HFS (⊿BOLD). The voxel-level correlation map was overlaid onto the fMRI activation surface map (Fig. 2BCD). Tic reduction correlated with a complex pattern of both increases and decreases in BOLD signals. Positive correlations represent reductions in tics correlating

with increases in BOLD and negative correlations represent reductions in tics correlating with decreases in BOLD. In subcortical regions, negative correlations were found in the PT and NAc (IL/RH) (Fig. 2B). Positive correlations were observed in the cerebellum spanning deep cerebellar nuclei and lobules IV and V (CL/LH) (Fig. 2C). For cortical regions (Fig. 2D), positive correlations were observed in the frontal cortex that include PFC, ACC, and OFC (IL/RH). The sensorimotor cortex corresponding to the hand, arm, and shoulder areas also showed a positive correlation (IL/RH). In addition, a wide range of parietal and occipital lobe regions showed positive correlations (IL/RH and CL/LH). In contrast, a negative correlation was seen in the medial frontal cortex containing Brodmann's area 8 and insula (IL/RH). Wernicke's area in the inferior parietal cortex also exhibited a negative correlation (CL/LH). Areas in the temporal lobe showed mixed effects of both positive and negative correlations (IL/RH). The gray matter and white matter voxel-level correlation surface maps and fMRI activation surface maps are shown for anatomical confirmation in supplementary Figs. S3 and S4.

ROI-level correlation analysis was performed, as it would be less sensitive in spatial specificity compared to voxel-level analysis, but would have more representative values within the ROI (Table 1, regions showing significant correlations in bold font). Consistent with voxel-level results, ACC, OFC, and occipital lobe showed positive correlations. ROI-level results revealed both positive and negative correlations in multiple temporal lobe regions (IL/RH and CL/LH), and positive correlations in the thalamus (IL/RH and CL/LH) and AM/NAc area (CL/LH). In contrast, ROI-level insula (IL/RH) showed a positive correlation inconsistent with voxel-level results (negative correlation).

3.3. Differential motor and limbic circuitry involvement in motor versus vocal tic production

We have previously shown in the TS-NHP model that disinhibition of neural activity in the sensorimotor striatum (PT), via microinfusion of the GABA$_A$ antagonist bicuculline, induced motor tics in the orofacial region and/or the arm region, absence of vocal tics. In contrast, pharmacological disinhibition of the NAc (limbic) induced vocal tics that primarily expressed as repetitive grunts (McCairn et al., 2016). Regional cerebral blood flow (rCBF) PET imaging revealed that activation in M1 and the cerebellum showed significantly greater activation during motor tic production than during vocal tic production ($t > 5.47$, corrected $p < 0.05$) (Fig. S1A). In contrast, the ACC, AM, and HP was significantly greater during vocal tic production than during motor tic production ($t > 5.47$, corrected $p < 0.05$) (Fig. S1B). Similarly, regional BOLD changes induced by thalamic HFS in the TS participants closely overlapped with the bicuculline-induced motor and vocal tic changes in regional rCBF in the NHP brain, where the brain areas of motor and vocal tic activity were affected by thalamic HFS (Fig. S1C).

3.4. Motor and vocal tic reduction by different circuit effects

Differences in motor versus vocal tic reduction, as represented in the correlation map, were further investigated and found that there were distinct differences in the activation patterns. There was a negative correlation between motor tic reduction and BOLD signal in the sensorimotor cortex, insula, and BD 8 (IL/RH) (Fig. 3A). In contrast, there was a negative correlation between vocal tic reduction and BOLD signal in the ACC in both hemispheres, and in the ipsilateral, right hemisphere's NAc and temporal lobe (IL/RH) (Fig. 3B). Of note, these differential motor and vocal tic network effects are consistent with the NHP-TS results (Fig. S1ab). In the present study, both motor and vocal tic reductions had negative correlations with activation specific to the superior region of Wernicke's area in the inferior parietal cortex (CL/LH) (Fig. 3AB). In addition, in the sensorimotor strip, vocal tic reduction correlated positively with BOLD generally covering the whole strip

Table 1

Thalamic HFS-Evoked BOLD Signals and Tic Reduction Correlation (ROI-level).

Regions	Volume mm^3	Coordinates (x, y, z)	Max t-Score	Correlation coefficient
Cerebellar				
IL cerebellum	1104	−15, +61, −16	+4.91	+0.42
CL cerebellum	**6072**	**+9, +57, −22**	**+6.25**	**+0.63***
Cortices and gyri				
IL/CL cuneus/precuneus/isthmus cingulate cortices	4584	+1, +71, +20	+7.19	−0.48
IL/CL caudal/rostral anterior cingulate cortices	2920	−9, −31, +6	−4.44	+0.08
IL/CL anterior cingulate/medial orbitofrontal cortices	**1048**	**−11, −51, +4**	**−2.64**	**+0.66***
IL lateral orbitofrontal cortex	**744**	**−41, −17, −12**	**−4.04**	**+0.86***
CL lateral orbitofrontal cortex	1696	−43, −37, −6	−2.32	+0.18
IL medial frontal gyrus	1208	−7, −25, +44	−3.13	−0.32
IL insula	**824**	**−41, −15, −4**	**−4.32**	**+0.65***
IL lateral occipital/lingual/pericalcarine gyri	2640	−9, +69, +8	+4.94	+0.43
CL lateral occipital/lingual/pericalcarine gyri	**2448**	**+17, +65, −12**	**+6.29**	**+0.58***
IL inferior parietal cortex	312	−45, +55, +18	+2.85	+0.22
CL inferior parietal cortex	2160	+39, +53, +26	+2.62	−0.26
CL superior parietal cortex	304	+11, +67, +50	+4.85	+0.30
IL sensorimotor cortex	9696	−49, +11, +28	+4.26	+0.29
IL superior/medial/inferior temporal cortices	**1496**	**−39, −5, −14**	**−4.70**	**+0.79***
CL superior temporal/pars orbitalis cortices	**1208**	**+39, −21, −12**	**−2.94**	**+0.74***
IL inferior temporal gyrus	**1488**	**−41, +7, −22**	**+3.36**	**−0.86***
Subcortical structures				
IL caudate/pallidum/putamen	3384	−15, +1, +22	−5.53	−0.23
CL caudate/pallidum/putamen	1992	+19, +7, +16	−4.77	−0.11
IL/CL thalamus	**3480**	**−13, +23, +8**	**+9.94**	**+0.63***
IL amygdala/accumbens area	392	−29, +9, −10	−6.34	−0.18
CL amygdala/accumbens area	**1272**	**+5, −5, −14**	**−3.74**	**+0.80***
Brain stem	2088	−1, +21, −18	+6.97	−0.18

Regions showing significant correlations in **bold** (* FWE-corrected p < 0.05). Abbreviations: BOLD, blood-oxygen-level dependent; CL, contralateral to the injection/stimulation site; HFS, high frequency stimulation; IL, ipsilateral to the injection/stimulation site; ROI, region of interest.

specifically including the face area, while motor tic reduction correlated negatively with BOLD only in the hand, arm, and shoulder areas. There were also a wide range of both positive and negative correlations among motor and vocal tic reduction and parietal and occipital lobe BOLD signal.

4. Discussion

The present results support the premise that TS is not simply due to a focal disorder in the brain, but rather the tic state is associated with large scale network abnormalities that are consistent across individuals with TS (Caligiore et al., 2017) and supported by findings in animal models (McCairn et al., 2009, 2013a, 2016). In addition, these same networks, both motor and limbic, are shown to be modulated by thalamic HFS in a symptom/network specific manner, and that these modulations strongly correlate with symptom improvement.

The application of brain imaging techniques and surgical interventions in individuals with TS and basic investigations in animal models have provided data into understanding the pathophysiology of TS (for review see (Hashemiyoon et al., 2017; Robertson et al., 2017; Testini et al., 2016a). Some important insights have come from NHP studies which have demonstrated that TS-like behavioral symptoms are associated with discrete neural networks (Grabli et al., 2004; Worbe et al., 2013) and these behaviors are underlined by specific, abnormal firing patterns within the BGCTC. Metabolic and electrophysiological studies have identified dysrhythmia in the BGCTC network during evoked motor tics with notable local field potential spikes and temporal coding of single-unit activity in the BG, cerebellum, and M1 (McCairn et al., 2009, 2013b). Vocal tics evoked by bicuculline-induced disinhibition of the NAc correlated with wide brain increases in measured blood flow on rCBF PET imaging in the limbic network that involved the ACC, AM, and HP (McCairn et al., 2016), with similar activity being reported for limbic pallidal disinhibition in anesthetized NHPs (Galineau et al., 2017). Similar electrophysiological abnormalities have been shown in

the local field potential recordings in cortical BG recipient regions of the NAc. Enhanced coupling between subcortical and cortical regions were also associated with phase-phase coupling, especially in alpha brain wave activity (7–12 Hz) (McCairn et al., 2016).

The results from the present study add to a growing body of evidence that TS should be considered a disorder of large scale cortical and subcortical global networks (Caligiore et al., 2017; McCairn et al., 2013b). Traditionally TS was conceived as a focal disorder, relating to abnormal dopamine levels in the striatum, and subsequent dysregulation of action selection via indirect and direct pathways of the BG (McNaught and Mink, 2011). Notable recent studies have revealed distinct cortical motor network pathology, for example, thinning of sensorimotor cortex in children with TS relative to controls (Sowell et al., 2008), abnormally enhanced structural connectivity between sensorimotor cortex, thalamus, and striatum (Worbe et al., 2015), observations of reduced intracortical inhibition within the motor cortex (Ziemann et al., 1997) and altered task-specific sensorimotor cortex activation (Thomalla et al., 2014), which lends credence to the global network dysrhythmia hypothesis.

While recent studies in rodents has demonstrated that interactions between the PT and motor cortex determine where (PT) and when (motor cortex) tics will occur (Israelashvili and Bar-Gad, 2015; Yael et al., 2016), our results also support an extended network model and replicate previous findings showing significant activation/abnormality of the cerebellum during the production of tics (Bohlhalter et al., 2006; Lerner et al., 2007; Stern et al., 2000), and that the cerebellum is an integral part of the tic generating network. The cerebellum is known to have direct and indirect connections with the BG via intralaminar thalamic nuclei (Hoshi et al., 2005). Therefore, it is possible that thalamic stimulation may directly activate the cerebellum or activate it indirectly through BG output and/or activation of cortico-cerebellar projections.

Tic reduction correlated with reduced activation in the striatum ipsilateral to stimulation. This result, perhaps not surprising, given the
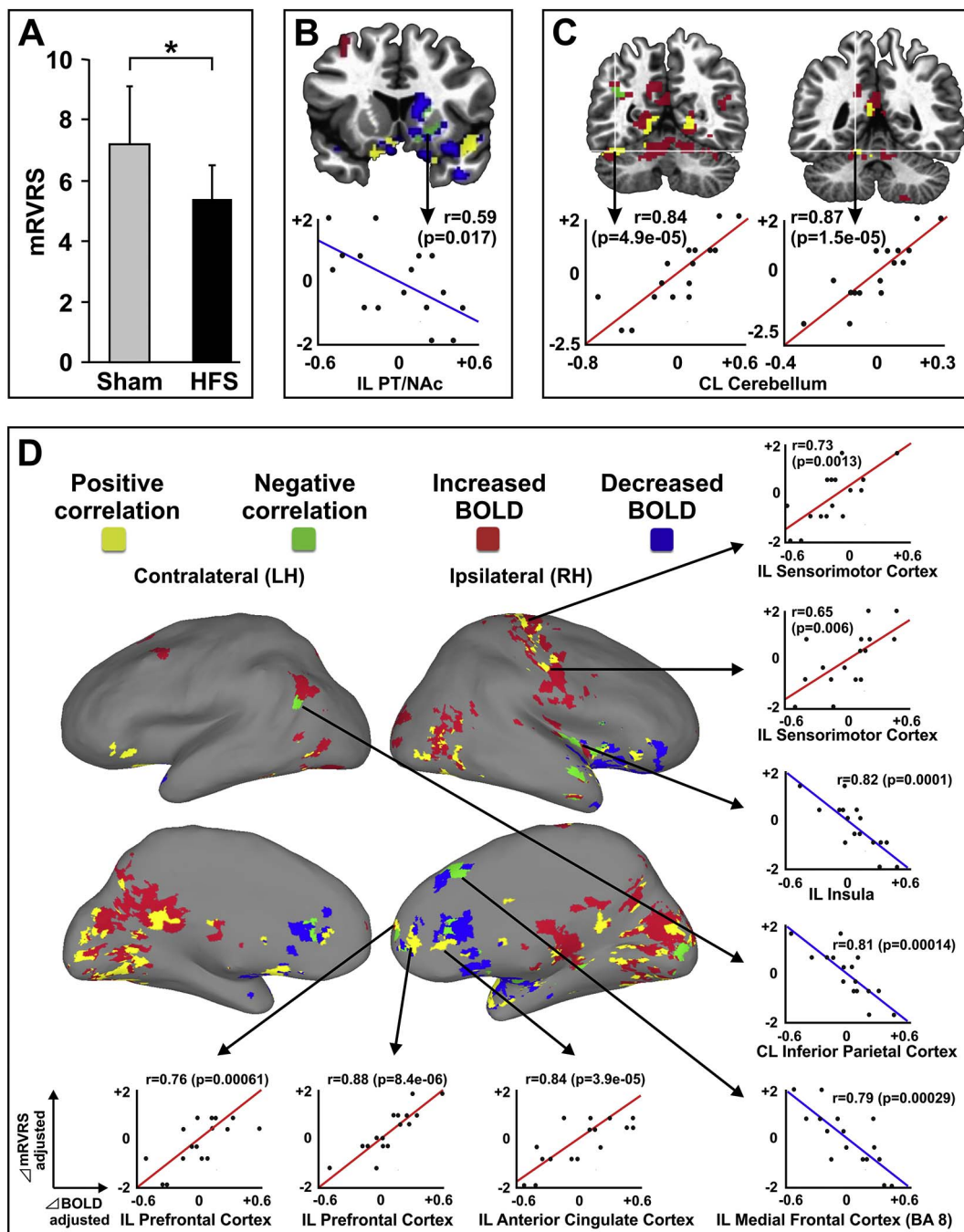
Fig. 2. Neural correlates of tic reduction by thalamic HFS. (A) Thalamic HFS resulted in lowering the mean mRVRS score (5.38 SEM ± 1.14) compared to no (sham) stimulation (mean mRVRS score of 7.25 SEM ± 1.98; p < 0.05). (B) In subcortical structures, thalamic HFS resulted in reductions in tics correlating with decreases in BOLD (negative correlations) in the PT and NAc (IL/RH), and (C) reductions in tics correlating with increases in BOLD (positive correlation) in the cerebellum spanning deep cerebellar nuclei and lobules IV and V (CL/LH). (D) In cortical structures, tic reduction positively correlated with BOLD signals in the frontal cortex, including PFC, ACC, OFC, sensorimotor cortex corresponding to the hand, arm, and shoulder areas (IL/RH), and a wide range of parietal and occipital lobe regions (IL/RH and CL/LH). In contrast, tic reduction negatively correlated with BOLD signals in the medial frontal cortex (Brodmann's area 8), and insula (IL/RH), and Wernicke's area (CL/LH). Abbreviations: ACC, anterior cingulate cortex; BA 8, Brodmann's area 8; NAc, nucleus accumbens; PT, putamen; OFC, orbitofrontal cortex; PFC, prefrontal cortex; BOLD, blood-oxygen-level dependent; HFS, high frequency stimulation; mRVRS, modified Rush Video Rating Scale, CL/LH, contralateral to the stimulation site in the left hemisphere; IL/RH, ipsilateral to the stimulation site in the right hemisphere; LH, left hemisphere; RH, right hemisphere.

pervasive striatal projections originating in thalamic CMPf, supports the premise that CMPf stimulation can modulate ongoing striatal activity (Kim et al., 2013). Individuals with TS display reduced striatal inter-neuron density (Kalanithi et al., 2005; Kataoka et al., 2010), and se-lective inhibition of striatal interneuron activity has been shown to lead to TS-like behavior in NHP (McCairn et al., 2009). Previous studies have shown that stimulation of the CMPf can induce excitatory, as well as inhibitory, responses in the striatum (Nanda et al., 2009). In

addition, electrical activation of the CMPf has been shown to induce GABAergic inhibition of striatal acetylcholine release (Zackheim and Abercrombie, 2005).

Since projections from the CMPf are topographically organized and span motor, limbic, and associative portions of the striatum, one might predict that stimulation would induce downstream effects on cortical areas in each of these categories. Previous neuroimaging studies have shown hyperactive metabolism in a range of motor, associative, and
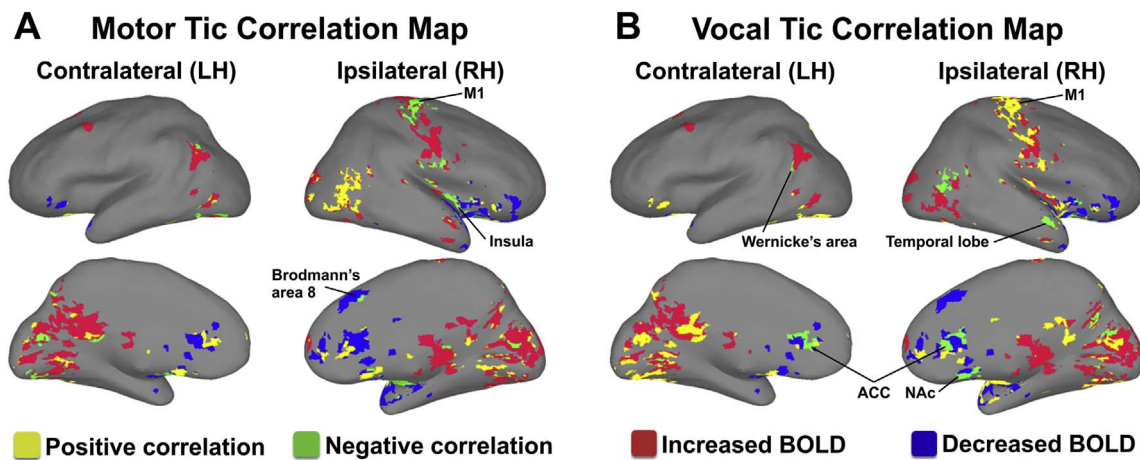
Fig. 3. Motor and vocal tic reduction by different circuit effects. (A) Negative correlations between motor tic reduction and BOLD signals in the sensorimotor cortex, insula, and Brodmann's area 8 (IL/RH) and superior region of Wernicke's area (CL/LH). (B) Negative correlations between vocal tic reduction and BOLD signals in the ACC of both hemispheres, NAc and temporal lobe (IL/RH), and inferior region of Wernicke's area (CL/LH). In addition, in the sensorimotor strip, vocal tic reduction correlated positively with BOLD generally covering the whole strip specifically including the face area, while motor tic reduction correlated negatively with BOLD only in the hand, arm, and shoulder areas. Both positive and negative correlations were found for motor and vocal tic reduction and parietal and occipital lobe BOLD signal. Abbreviations: ACC, anterior cingulate cortex; NAc, nucleus accumbens; BOLD, blood-oxygen-level dependent; CL/LH, contralateral to the stimulation site in the left hemisphere; IL/RH, ipsilateral to the stimulation site in the right hemisphere; LH, left hemisphere; RH, right hemisphere.

limbic regions in TS (Bohlhalter et al., 2006; Lerner et al., 2007; Pourfar et al., 2011). The present study suggests that many of these regions, which include premotor and sensorimotor cortex, insula, temporal lobe, cingulate, and somatosensory association areas, are modulated by thalamic stimulation (Kim et al., 2013). In addition, there are hypotheses linking the insula, ACC, and PFC to TS mechanisms mediating premonitory urge (Cavanna et al., 2017; Hallett, 2015). Indeed, insula, ACC, and PFC activation have been shown to be correlated to premonitory urges as assessed in subjects undergoing a blink suppression test (Berman et al., 2012; Cavanna et al., 2017; Lerner et al., 2009). While resting state fMRI studies on TS show increased connectivity in the insula and the sensorimotor cortex (Tinaz et al., 2014), the present results also show that tic reduction highly correlates with the BOLD signal changes in those areas, especially with motor tics. Therefore, thalamic stimulation might act through the insula and sensorimotor cortices to affect the premonitory urge-related motor tic response.

Some technical limitations must be considered for the results of this study. First, anesthesia may influence the DBS-evoked BOLD signal because patients received both inhaled halogenated ether anesthetic and intravenous fentanyl during fMRI acquisition. Second, the DBS electrode created a susceptibility artifact that reduced the strength of the BOLD signal along the electrode trajectory (In et al., 2017). The artifact could lead to an underestimation of DBS-evoked BOLD in the immediate vicinity of the electrodes, which may have affected the results of our correlation analyses within that region.

5. Conclusion

Overall, the present study shows that thalamic HFS in TS participants has wide-ranging effects that impact the frontostriatal, limbic, and motor networks. These findings suggest that thalamic HFS may suppress striatal output and reduce tic production via downstream effects in both the frontal and motor cortices. Furthermore, the present results suggest that the suppression of the motor and insula networks correlate with motor tic reduction, whereas suppression of frontal and parietal networks correlate with vocal tic reduction, implying it would be a critical factor to modulate both frontostriatal and motor networks for treatment of TS. Our study also provides unique translational information supporting the NHP-TS model. Future studies in clinical and preclinical research will be necessary to identify whether these network changes are cause or effect of TS symptoms.

Appendix A. Supplementary data

Supplementary data to this article can be found online at https://doi.org/10.1016/j.nicl.2018.02.018.

References

Ackermans, L., Duits, A., van der Linden, C., Tijssen, M., Schruers, K., Temel, Y., Kleijer, M., Nederveen, P., Bruggeman, R., Tromp, S., van Kranen-Mastenbroek, V., Kingma, H., Cath, D., Visser-Vandewalle, V., 2011. Double-blind clinical trial of thalamic stimulation in patients with Tourette syndrome. Brain 134, 832–844.

Albin, R.L., Mink, J.W., 2006. Recent advances in Tourette syndrome research. Trends Neurosci. 29, 175–182.

Association, A.P., 2013. Diagnostic and Statistical Manual of Mental Disorders, Fifth Edition, DSM-5. American Psychiatric Association, Arlington, VA.

Berendse, H.W., Groenewegen, H.J., 1991. Restricted cortical termination fields of the midline and intralaminar thalamic nuclei in the rat. Neuroscience 42, 73–102.

Berman, B.D., Horovitz, S.G., Morel, B., Hallett, M., 2012. Neural correlates of blink suppression and the buildup of a natural bodily urge. NeuroImage 59, 1441–1450.

Bohlhalter, S., Goldfine, A., Matteson, S., Garraux, G., Hanakawa, T., Kansaku, K., Wurzman, R., Hallett, M., 2006. Neural correlates of tic generation in Tourette syndrome: an event-related functional MRI study. Brain 129, 2029–2037.

Caligiore, D., Mannella, F., Arbib, M.A., Baldassarre, G., 2017. Dysfunctions of the basal ganglia-cerebellar-thalamo-cortical system produce motor tics in Tourette syndrome. PLoS Comput. Biol. 13, e1005395.

Cavanna, A.E., Black, K.J., Hallett, M., Voon, V., 2017. Neurobiology of the premonitory urge in Tourette's syndrome: pathophysiology and treatment implications. J. Neuropsychiatr. Clin. Neurosci. 29, 95–104.

Cavdar, S., Onat, F.Y., Cakmak, Y.O., Yananli, H.R., Gulcebi, M., Aker, R., 2008. The pathways connecting the hippocampal formation, the thalamic reuniens nucleus and the thalamic reticular nucleus in the rat. J. Anat. 212, 249–256.

Chen, G., Adleman, N.E., Saad, Z.S., Leibenluft, E., Cox, R.W., 2014. Applications of multivariate modeling to neuroimaging group analysis: a comprehensive alternative to univariate general linear model. NeuroImage 99, 571–588.

Cox, R.W., 1996. AFNI: software for analysis and visualization of functional magnetic resonance neuroimages. Comput. Biomed. Res. 29, 162–173.

Cox, R.W., Jesmanowicz, A., 1999. Real-time 3D image registration for functional MRI. Magn. Reson. Med. 42, 1014–1018.

Crossley, E., Cavanna, A.E., 2013. Sensory phenomena: clinical correlates and impact on quality of life in adult patients with Tourette syndrome. Psychiatry Res. 209, 705–710.

Da Cunha, C., Boschen, S.L., Gomez, A.A., Ross, E.K., Gibson, W.S., Min, H.K., Lee, K.H., Blaha, C.D., 2015. Toward sophisticated basal ganglia neuromodulation: review on basal ganglia deep brain stimulation. Neurosci. Biobehav. Rev. 58, 186–210.

Eckert, U., Metzger, C.D., Buchmann, J.E., Kaufmann, J., Osoba, A., Li, M., Safron, A., Liao, W., Steiner, J., Bogerts, B., Walter, M., 2012. Preferential networks of the mediodorsal nucleus and centromedian-parafascicular complex of the thalamus-A DTI tractography study. Hum. Brain Mapp. 33, 2627–2637.

Eickhoff, S.B., Paus, T., Caspers, S., Grosbras, M.H., Evans, A.C., Zilles, K., Amunts, K., 2007. Assignment of functional activations to probabilistic cytoarchitectonic areas revisited. NeuroImage 36, 511–521.

Fischl, B., 2012. FreeSurfer. NeuroImage 62, 774–781.

Galineau, L., Kas, A., Worbe, Y., Chaigneau, M., Herard, A.S., Guillermier, M., Delzescaux, T., Feger, J., Hantraye, P., Tremblay, L., 2017. Cortical areas involved in behavioral expression of external pallidum dysfunctions: a PET imaging study in non-human primates. NeuroImage 146, 1025–1037.

Gibson, W.S., Jo, H.J., Testini, P., Cho, S., Felmlee, J.P., Welker, K.M., Klassen, B.T., Min, H.K., Lee, K.H., 2016. Functional correlates of the therapeutic and adverse effects evoked by thalamic stimulation for essential tremor. Brain 139, 2198–2210.

Goetz, C.G., Pappert, E.J., Louis, E.D., Raman, R., Leurgans, S., 1999. Advantages of a modified scoring method for the rush video-based tic rating scale. Mov. Disord. 14, 502–506.

Gorny, K.R., Presti, M.F., Goerss, S.J., Hwang, S.C., Jang, D.P., Kim, I., Min, H.K., Shu, Y., Favazza, C.P., Lee, K.H., Bernstein, M.A., 2013. Measurements of RF heating during 3.0-T MRI of a pig implanted with deep brain stimulator. Magn. Reson. Imaging 31, 783–788.

Gotts, S.J., Jo, H.J., Wallace, G.L., Saad, Z.S., Cox, R.W., Martin, A., 2013. Two distinct forms of functional lateralization in the human brain. Proc. Natl. Acad. Sci. U. S. A. 110, E3435–3444.

Grabli, D., McCairn, K., Hirsch, E.C., Agid, Y., Feger, J., Francois, C., Tremblay, L., 2004. Behavioural disorders induced by external globus pallidus dysfunction in primates: I. Behavioural study. Brain 127, 2039–2054.

Hallett, M., 2001. Neurophysiology of tics. Adv. Neurol. 85, 237–244.

Hallett, M., 2015. Tourette syndrome: update. Brain Dev. 37, 651–655.

Hashemiyoon, R., Kuhn, J., Visser-Vandewalle, V., 2017. Putting the pieces together in Gilles de la Tourette syndrome: exploring the link between clinical observations and the biological basis of dysfunction. Brain Topogr. 30, 3–29.

Holmes, C.J., Hoge, R., Collins, L., Woods, R., Toga, A.W., Evans, A.C., 1998. Enhancement of MR images using registration for signal averaging. J. Comput. Assist. Tomogr. 22, 324–333.

Hoshi, E., Tremblay, L., Feger, J., Carras, P.L., Strick, P.L., 2005. The cerebellum communicates with the basal ganglia. Nat. Neurosci. 8, 1491–1493.

Huys, D., Bartsch, C., Koester, P., Lenartz, D., Maarouf, M., Daumann, J., Mai, J.K., Klosterkotter, J., Hunsche, S., Visser-Vandewalle, V., Woopen, C., Timmermann, L., Sturm, V., Kuhn, J., 2016. Motor improvement and emotional stabilization in patients with Tourette syndrome after deep brain stimulation of the ventral anterior and ventrolateral motor part of the thalamus. Biol. Psychiatry 79, 392–401.

In, M.H., Cho, S., Shu, Y., Min, H.K., Bernstein, M.A., Speck, O., Lee, K.H., Jo, H.J., 2017. Correction of metal-induced susceptibility artifacts for functional MRI during deep brain stimulation. NeuroImage 158, 26–36.

Israelashvili, M., Bar-Gad, I., 2015. Corticostriatal divergent function in determining the temporal and spatial properties of motor tics. J. Neurosci. 35, 16340–16351.

Jayaraman, A., 1985. Organization of thalamic projections in the nucleus accumbens and the caudate nucleus in cats and its relation with hippocampal and other subcortical afferents. J. Comp. Neurol. 231, 396–420.

Kalanithi, P.S., Zheng, W., Kataoka, Y., DiFiglia, M., Grantz, H., Saper, C.B., Schwartz, M.L., Leckman, J.F., Vaccarino, F.M., 2005. Altered parvalbumin-positive neuron distribution in basal ganglia of individuals with Tourette syndrome. Proc. Natl. Acad. Sci. U. S. A. 102, 13307–13312.

Kataoka, Y., Kalanithi, P.S., Grantz, H., Schwartz, M.L., Saper, C., Leckman, J.F., Vaccarino, F.M., 2010. Decreased number of parvalbumin and cholinergic interneurons in the striatum of individuals with Tourette syndrome. J. Comp. Neurol. 518, 277–291.

Kim, J.P., Min, H.K., Knight, E.J., Duffy, P.S., Abulseoud, O.A., Marsh, M.P., Kelsey, K., Blaha, C.D., Bennet, K.E., Frye, M.A., Lee, K.H., 2013. Centromedian-parafascicular deep brain stimulation induces differential functional inhibition of the motor, associative, and limbic circuits in large animals. Biol. Psychiatry 74, 917–926.

Knight, E.J., Testini, P., Min, H.K., Gibson, W.S., Gorny, K.R., Favazza, C.P., Felmlee, J.P., Kim, I., Welker, K.M., Clayton, D.A., Klassen, B.T., Chang, S.Y., Lee, K.H., 2015. Motor and nonmotor circuitry activation induced by subthalamic nucleus deep brain stimulation in patients with Parkinson disease: Intraoperative functional magnetic resonance imaging for deep brain stimulation. Mayo Clin. Proc. 90, 773–785.

Krack, P., Hariz, M.I., Baunez, C., Guridi, J., Obeso, J.A., 2010. Deep brain stimulation: from neurology to psychiatry? Trends Neurosci. 33, 474–484.

Kringelbach, M.L., Jenkinson, N., Owen, S.L., Aziz, T.Z., 2007. Translational principles of deep brain stimulation. Nat. Rev. Neurosci. 8, 623–635.

Lerner, A., Bagic, A., Boudreau, E.A., Hanakawa, T., Pagan, F., Mari, Z., Bara-Jimenez, W., Aksu, M., Garraux, G., Simmons, J.M., Sato, S., Murphy, D.L., Hallett, M., 2007. Neuroimaging of neuronal circuits involved in tic generation in patients with Tourette syndrome. Neurology 68, 1979–1987.

Lerner, A., Bagic, A., Hanakawa, T., Boudreau, E.A., Pagan, F., Mari, Z., Bara-Jimenez, W., Aksu, M., Sato, S., Murphy, D.L., Hallett, M., 2009. Involvement of insula and cingulate cortices in control and suppression of natural urges. Cereb. Cortex 19, 218–223.

Macchi, G., Bentivoglio, M., Molinari, M., Minciacchi, D., 1984. The thalamo-caudate versus thalamo-cortical projections as studied in the cat with fluorescent retrograde double labeling. Exp. Brain Res. 54, 225–239.

Maciunas, R.J., Maddux, B.N., Riley, D.E., Whitney, C.M., Schoenberg, M.R., Ogrocki, P.J., Albert, J.M., Gould, D.J., 2007. Prospective randomized double-blind trial of bilateral thalamic deep brain stimulation in adults with Tourette syndrome. J. Neurosurg. 107, 1004–1014.

McCairn, K.W., Bronfeld, M., Belelovsky, K., Bar-Gad, I., 2009. The neurophysiological correlates of motor tics following focal striatal disinhibition. Brain 132, 2125–2138.

McCairn, K.W., Iriki, A., Isoda, M., 2013a. Deep brain stimulation reduces Tic-related neural activity via temporal locking with stimulus pulses. J. Neurosci. 33, 6581–6593.

McCairn, K.W., Iriki, A., Isoda, M., 2013b. Global dysrhythmia of cerebro-basal ganglia-cerebellar networks underlies motor tics following striatal disinhibition. J. Neurosci. 33, 697–708.

McCairn, K.W., Iriki, A., Isoda, M., 2015. Common therapeutic mechanisms of pallidal deep brain stimulation for hypo- and hyperkinetic movement disorders. J. Neurophysiol. 114, 2090–2104.

McCairn, K.W., Nagai, Y., Hori, Y., Ninomiya, T., Kikuchi, E., Lee, J.Y., Suhara, T., Iriki, A., Minamimoto, T., Takada, M., Isoda, M., Matsumoto, M., 2016. A primary role for nucleus accumbens and related limbic network in vocal tics. Neuron 89, 300–307.

McGuire, J.F., McBride, N., Piacentini, J., Johnco, C., Lewin, A.B., Murphy, T.K., Storch, E.A., 2016. The premonitory urge revisited: an individualized premonitory urge for tics scale. J. Psychiatr. Res. 83, 176–183.

McNaught, K.S., Mink, J.W., 2011. Advances in understanding and treatment of Tourette syndrome. Nat. Rev. Neurol. 7, 667–676.

Nanda, B., Galvan, A., Smith, Y., Wichmann, T., 2009. Effects of stimulation of the centromedian nucleus of the thalamus on the activity of striatal cells in awake rhesus monkeys. Eur. J. Neurosci. 29, 588–598.

Ottersen, O.P., 1981. Afferent connections to the amygdaloid complex of the rat with some observations in the cat. III. Afferents from the lower brain stem. J. Comp. Neurol. 202, 335–356.

Pourfar, M., Feigin, A., Tang, C.C., Carbon-Correll, M., Bussa, M., Budman, C., Dhawan, V., Eidelberg, D., 2011. Abnormal metabolic brain networks in Tourette syndrome. Neurology 76, 944–952.

Robertson, M.M., Eapen, V., Singer, H.S., Martino, D., Scharf, J.M., Paschou, P., Roessner, V., Woods, D.W., Hariz, M., Mathews, C.A., Crncec, R., Leckman, J.F., 2017. Gilles de la Tourette syndrome. Nat. Rev. Dis. Prim. 3, 16097.

Saad, Z.S., Glen, D.R., Chen, G., Beauchamp, M.S., Desai, R., Cox, R.W., 2009. A new method for improving functional-to-structural MRI alignment using local Pearson correlation. NeuroImage 44, 839–848.

Sadikot, A.F., Rymar, V.V., 2009. The primate centromedian-parafascicular complex: anatomical organization with a note on neuromodulation. Brain Res. Bull. 78, 122–130.

Schaltenbrand, G., Wahren, W., 1977. Atlas for Stereotaxy of the Human Brain: Architectonic Organisation of the Thalamic Nuclei by Rolf Hassler. Georg Thieme Publishers, Stuttgart.

Sowell, E.R., Kan, E., Yoshii, J., Thompson, P.M., Bansal, R., Xu, D., Toga, A.W., Peterson, B.S., 2008. Thinning of sensorimotor cortices in children with Tourette syndrome. Nat. Neurosci. 11, 637–639.

Stern, E., Silbersweig, D.A., Chee, K.Y., Holmes, A., Robertson, M.M., Trimble, M., Frith, C.D., Frackowiak, R.S., Dolan, R.J., 2000. A functional neuroanatomy of tics in Tourette syndrome. Arch. Gen. Psychiatry 57, 741–748.

Testini, P., Min, H.K., Bashir, A., Lee, K.H., 2016a. Deep brain stimulation for Tourette's syndrome: the case for targeting the thalamic centromedian-parafascicular complex. Front. Neurol. 7, 193.

Testini, P., Zhao, C.Z., Stead, M., Duffy, P.S., Klassen, B.T., Lee, K.H., 2016b. Centromedian-parafascicular complex deep brain stimulation for Tourette syndrome: a retrospective study. Mayo Clin. Proc. 91, 218–225.

Thomalla, G., Jonas, M., Baumer, T., Siebner, H.R., Biermann-Ruben, K., Ganos, C., Orth, M., Hummel, F.C., Gerloff, C., Muller-Vahl, K., Schnitzler, A., Munchau, A., 2014. Costs of control: decreased motor cortex engagement during a Go/NoGo task in Tourette's syndrome. Brain 137, 122–136.

Tinaz, S., Belluscio, B.A., Malone, P., van der Veen, J.W., Hallett, M., Horovitz, S.G., 2014. Role of the sensorimotor cortex in Tourette syndrome using multimodal imaging. Hum. Brain Mapp. 35, 5834–5846.

Van der Werf, Y.D., Witter, M.P., Groenewegen, H.J., 2002. The intralaminar and midline nuclei of the thalamus. Anatomical and functional evidence for participation in processes of arousal and awareness. Brain Res. Brain Res. Rev. 39, 107–140.

Vandewalle, V., van der Linden, C., Groenewegen, H.J., Caemaert, J., 1999. Stereotactic treatment of Gilles de la Tourette syndrome by high frequency stimulation of thalamus. Lancet 353, 724.

Worbe, Y., Sgambato-Faure, V., Epinat, J., Chaigneau, M., Tande, D., Francois, C., Feger, J., Tremblay, L., 2013. Towards a primate model of Gilles de la Tourette syndrome: anatomo-behavioural correlation of disorders induced by striatal dysfunction. Cortex 49, 1126–1140.

Worbe, Y., Marrakchi-Kacem, L., Lecomte, S., Valabregue, R., Poupon, F., Guevara, P., Tucholka, A., Mangin, J.F., Vidailhet, M., Lehericy, S., Hartmann, A., Poupon, C., 2015. Altered structural connectivity of cortico-striato-pallido-thalamic networks in Gilles de la Tourette syndrome. Brain 138, 472–482.

Yael, D., Israelashvili, M., Bar-Gad, I., 2016. Animal models of Tourette syndrome-from proliferation to standardization. Front. Neurosci. 10, 132.

Zackheim, J., Abercrombie, E.D., 2005. Thalamic regulation of striatal acetylcholine efflux is both direct and indirect and qualitatively altered in the dopamine-depleted striatum. Neuroscience 131, 423–436.

Ziemann, U., Winter, M., Reimers, C.D., Reimers, K., Tergau, F., Paulus, W., 1997. Impaired motor cortex inhibition in patients with amyotrophic lateral sclerosis. Evidence from paired transcranial magnetic stimulation. Neurology 49, 1292–1298.